Evolutionarily Optimized Electromagnetic Sensor Measurements for Robust Surgical Navigation

Xiongbiao Luo, *Senior Member, IEEE*, Chaoyang Shi*, Hui-Qing Zeng*, Henry C. Ewurum, Ying Wan, Yingying Guo, Seang Pagnha, Xiao-Bin Zhang, Yan-Ping Du, and Xiangjian He

***Abstract*—Miniaturized electromagnetic sensors are increasingly introduced to navigate surgical instruments to anatomical targets during minimally invasive procedures such as endoscopic surgery. These sensors are usually attached at the distal tips of surgical instruments to track their three-dimensional motion represented by position and orientation in six degrees of freedom. Unfortunately, these sensors suffer from inaccurate measurements and jitter errors due to patient movement (e.g., respiratory motion) and magnetic field distortion. This paper proposes an evolutionary computing strategy to optimize the sensor measurements and improve the tracking accuracy of surgical navigation. We modified two evolutionary computation algorithms and proposed adaptive particle swarm optimization (APSO) and observation-boosted differential evolution (OBDE) to enhance the navigation accuracy. The experimental results demonstrate that our modified algorithms to evolutionarily optimize electromagnetic sensor measurements can critically reduce the tracking error from 4.8 mm to 2.9 mm. In particular, OBDE outperforms APSO for electromagnetic endoscopic navigation.**

***Index Terms*—Electromagnetic sensor, surgical tracking and navigation, evolutionary computation, particle swarm optimization, differential evolution, image-guided intervention**

I. Introduction

Electromagnetic (EM) tracking is widely used in simulation (e.g., military flight and gunnery simulation systems) and medical procedures [1], while it is a relatively new approach that locates disposable tools or sensors situated inside or outside the body in real time. The EM tracking system generally consists of several key components of an electronic unit, a magnetic field transmitter, and miniaturized EM sensors (Fig. 1). While the transmitter generates the optimal tracking volume to perceive 3-D position and orientation of EM sensors located inside the tracking volume, the electronic unit integrated with power supply from a personal computer tracks six degrees of freedom (6DoF) miniaturized EM sensors. Such an EM tracking system is particularly powerful for various surgical navigation applications, e.g., ultrasound image fusion, biopsy needle guidance, oncology, and neurosurgery. More interestingly, EM tracking techniques also have been increasingly utilized to track and localize surgical continuum robots and intravascular flexible instruments in minimally invasive surgery because of their superior attributes of miniature sensor sizes and freedom of line-of-sight constraints [2].

To develop EM-based surgical navigation for image-guided intervention, miniaturized EM sensors must be embedded into medical instruments such as flexible endoscopes (e.g., bronchoscope and colonoscope) that are integrated with video cameras. After calibrating the EM sensor and surgical instrument coordinate systems (i.e., determining the spatial transformation between the EM sensor and surgical instrument), surgeons can intuitively locate and navigate the surgical instrument inside the body. While the EM tracking system provides real-time 3-D position and orientation information in 6DoF for locating surgical instruments during surgery, EM sensor measurements are still problematic. There are two main reasons behind this: (1) location sensitivity and (2) stochastic jitter error. The former results from any patient movement (i.e., respiratory motion, tissue deformation, or coughing). Since EM sensor outputs measure 3-D motion with 6DoF position and orientation information in a fixed world coordinate system, they do not correspond exactly to the current position and direction of the surgical instrument. This leads to inaccurate EM sensor measurements. The jitter error results from the tracking volume or magnetic field distortion caused by ferrous metals or conductive materials within or close to the tracking volume. While most surgical instruments contain metal materials, patient tables or other materials below them can distort the tracking volume. In general, the distortion of the tracking volume unavoidably results in unstable or jitter measurements.

This work aims to apply and compare two commonly established evolutionary computation algorithms including particle swarm optimization (PSO) and differential evolution (DE) to tackle the limitations of the EM tracking system and optimize EM sensor measurements. Since the performance of PSO and DE depends critically on their operators and evolutionary factors, we propose adaptive particle swarm optimization (APSO) and observation-boosted differential evolution (OBDE). Two highlights of this work are clarified: (1) modification of the standard PSO and DE algorithms by introducing the current EM sensor observation and (2) comparison of the proposed APSO and OBDE applied to surgical navigation.

The rest of this paper is organized as follows. Section II briefly reviews current work related to EM tracking. Section III modifies two evolutionary algorithms of PSO and DE, fol-

This work was in part supported by the Fundamental Research Funds for the Central Universities (Grant No. 20720180062) and National Natural Science Foundation of China (Grant No. 51520105006). *Asterisk indicates corresponding author*. X. Luo and Y. Wan contributed equally to this work.

X. Luo, H. Ewurum, Y. Guo, and S. Pagnha are with the Department of Computer Science, XMU Center for Surgery and Engineering, Xiamen University, Xiamen 361005, China, (e-mail: lurowan@outlook.com)

C. Shi is with the Key Lab for Mechanism Theory and Equipment Design of Ministry of Education, School of Mechanical Engineering, Tianjin University, Tianjin, 300072, China (e-mail: chaoyanghit@gmail.com)

X. Zhang, Y. Du, and H. Zeng are with the Zhongshan Hospital, Xiamen University, Xiamen 361004, China, (email: 13606080893@139.com)

Y. Wan and X. He are with the School of Computing and Communications, University of Technology Sydney, Australia (e-mail: joyee.wan@gmail.com)

(a) Electronic unit (b) Cubic transmitter (c) EM sensors

Fig. 1: An EM tracking system generally works in conjunction with an electronic unit, a magnetic field transmitter, and miniaturized EM sensors. The electronic unit typically controls the electromagnetic magnetic field transmitter that produces an electromagnetic tracking volume. EM sensors are perceived and localized by the tracking volume in accordance with the working principle of mutual induction. Image courtesy of Northern Digital Inc., Waterloo, Canada

lowed by applying them to optimize EM sensor measurements for surgical navigation in Section IV. Section VI shows and compares the experimental results obtained from different surgical electromagnetic navigation approaches. Section VII discusses the performance of the proposed methods and future work before summarizing this work in Section VIII.

II. Related Work

EM tracking systems suffer from various limitations (discussed above) associated with their working principles. While these systems are prone to produce measurement errors due to magnetic field distortions, especially in a dynamic clinical environment, they also suffer from a limited workspace and provide non-uniform measurement accuracy throughout the tracking volume. The highest and uniform accuracy is typically generated around the center of the tracking volume [3].

To tackle the EM limitations, numerous approaches have been proposed and discussed in the literature. Keeping metals or conductive materials away from the tracking volume is a simple and easy way to minimize the magnetic field distortion. However, this is somewhat unrealistic in the operating room. Moreover, hybrid tracking that combines EM tracking and 2-D/3-D registration techniques provides a promising way to resolve the limitations. Mori et al. [4] used the EM tracking results to initialize the optimizer of image registration. Soper et al. [5] integrated Kalman filtering with image registration to improve the performance of EM tracking. Reichl et al. [6] discussed a new tracking paradigm in accordance with electromagnetic servoing. Luo et al. [7] proposed an animated particle filtering method to fuse EM sensor outputs and endoscopic video images. More recently, Sadjadi et al. [8] compensated the dynamic field distortion of EM tracking using a simultaneous calibration strategy. While Sorger et al. [9] employed EM tracking for endobronchial ultrasound, Hofstad et al. [10], [11] improved the registration between the EM system and preoperative images. As an alternative to electromagnetic tracking, Shen et al. [12], [13] used depth estimation and recognition techniques to navigate the endoscope, while video summarization and classification were introduced to locate the endoscope [14], [15]. Additionally, a tabletop field generator (Northern Digital Inc., Waterloo, Canada) has been developed to incorporate a thin barrier that can minimize any tracking distortions caused by conductive or ferromagnetic materials. More recently, numerous researchers focus on improving the accuracy of EM tracking. Song et al. [16] introduced a strategy of rotating uniaxial coil with sparse points and closed form analytic solution to improve magnetic tracking. Liu et al. [17] compensated the geomagnetic vector measurement error for the differential magnetic field method. While Su et al. [18] investigated the link between the tracking distance and accuracy, Dai et al. [19] proposed a simple and efficient electromagnetic tracking approach that uses uniaxial transmitting coil and triaxial magneto-resistive sensor. All these methods improved the performance of EM tracking for various applications.

Generally speaking, EM trackers are dynamic systems that commonly produce inaccurate, noisy, or stochastic measurements (or observations). In this respect, global and stochastic optimization methods are required to deal with these dynamic measurements. This work is to address these limitations of EM trackers using evolutionary optimization or computation.

As a family of artificial intelligence, evolutionary computation employs biological evolution (e.g., mutation and natural selection) to solve dynamic optimization problems [20]. Evolutionary optimization includes various implementation algorithms, particularly particle swarm optimization [21] and differential evolution [22]. These algorithms have a meta-heuristic or stochastic optimization property and are increasingly introduced to practical applications such as image segmentation and object recognitions [23]. We modify these algorithms and enhance their performance to improve the accuracy of EM sensor measurements.

III. Approaches: Evolutionary Optimization

This section describes adaptive particle swarm optimization (APSO) and observation-boosted differential evolution (OBDE) and their application to evolutionarily optimize EM sensor outputs for improving surgical navigation.

Without loss of generality, we introduce some symbols. Evolutionary computation algorithms usually generate a population $\mathcal{X}$ of potential or random solutions (or called individuals) $\mathcal{X} = \{\mathbf{x}_{i,g} \in \mathcal{R}^D\}_{i=1,2,\cdots,N,\, g=1,2,\cdots,G}$, where N is the population size, G is the generation number, and D is

the dimension of individual or vector $\mathbf{x}_{i,g}$. These algorithms propagate the generated population at each iteration (also called generation g) to approximate the optimal solution of global and stochastic optimization problems.

Evolutionary optimization is usually driven by two primary forces of operation and selection. It is the operation force that employs different propagation strategies to evolve individuals, which also results in difference between the adaptive particle swarm optimization and observation-boosted differential evolution methods. Moreover, evolutionary factors have direct influence on the optimization performance. The following discusses adaptive particle swarm optimization, observation-boosted differential evolution, and their evolutionary factors.

A. Adaptive Particle Swarm Optimization

Compared to particle swarm optimization, adaptive particle swarm optimization introduces the current observation to precisely propagate individuals in the population, while the current observation is also used to calculate the fitness of the individual and adaptively determine evolutionary parameters at the current generation or iteration.

1) Individual Propagation: In particle swarm optimization, the i-th individual or vector $\mathbf{x}_{i,g-1}$ at generation $g-1$ is propagated to new individual $\mathbf{x}_{i,g}$ at generation g in accordance with the moving speed $\mathbf{a}_{i,g}$ by [21]:

$$\mathbf{x}_{i,g} = \mathbf{x}_{i,g-1} + \mathbf{a}_{i,g}, \tag{1}$$

$$\mathbf{a}_{i,g} = \omega \mathbf{a}_{i,g-1} + \varphi_b + \varphi_c, \tag{2}$$

$$\varphi_b = \mu_1 \eta_1 (\mathbf{b}_{i,g-1} - \mathbf{x}_{i,g-1}), \varphi_c = \mu_2 \eta_2 (\mathbf{c}_{g-1} - \mathbf{x}_{i,g-1}), \tag{3}$$

where inertial weight ω controls to preserve previous speed $\mathbf{a}_{i,g-1}$, cognitive factor μ_1 and μ_2 are acceleration constants, η_1 and η_2 yield the uniform distribution with the interval [0, 1], the local individual best $\mathbf{b}_{i,g-1}$ is the best candidate solution obtained by the i-th individual so far, and the global general best $\mathbf{c}_{g-1}$ is the best candidate solution selected from population $\mathcal{B}_{g-1} = \{\mathbf{b}_{i,g-1}\}_{i=1}^{N}$ at generation $g-1$.

Inertia term $\omega \mathbf{a}_{i,g-1}$ is used to keep the individual moving in the same direction it was originally heading to. Cognitive term φ_b memorizes the regions in the search space where the individual achieves large fitness and intends to return. Social term φ_c enables the individual to progress in the best region where the population has discovered so far at generation $g-1$.

2) Population Update: After propagating all the individuals at generation or iteration g, the local individual best $\mathbf{b}_{i,g}$ and the global general best $\mathbf{c}_g$ are updated by

$$\mathbf{b}_{i,g} = \begin{cases} \mathbf{x}_{i,g} & \text{if} f(\mathbf{x}_{i,g}) > f(\mathbf{b}_{i,g-1}) \\ \mathbf{b}_{i,g-1} & \text{otherwise} \end{cases}, \tag{4}$$

$$\mathbf{c}_g = \arg \max_{\mathbf{b}_{i,g} \in \mathcal{B}_g} f(\mathbf{b}_{i,g}). \tag{5}$$

where function $f(\cdot)$ is defined as the fitness of the individual to evaluate the performance of the new individual. Note that Eq. (4) compares the new individual $\mathbf{x}_{i,g}$ at generation g to the previous local individual best $\mathbf{b}_{i,g-1}$ because the individual propagation step does not guarantee that $\mathbf{x}_{i,g}$ is better than its corresponding individual $\mathbf{b}_{i,g-1}$. In this respect, the local individual best at generation g is selected between $\mathbf{x}_{i,g}$ and $\mathbf{b}_{i,g-1}$ on the basis of their fitness.

3) Adaptive Coefficients: The performance of particle swarm optimization depends critically on speed $\mathbf{a}_{i,g-1}$, fitness $f(\cdot)$ and user-provided coefficients ω, μ_1 and μ_2. The standard particle swarm optimization algorithm sets evolutionary parameters ω, μ_1 and μ_2 as pre-fixed constants. On the other hand, speed $\mathbf{a}_{i,g-1}$, and fitness $f(\cdot)$ are not associated with the current observation during optimization.

Our idea is to introduce the current observation to determine speed $\mathbf{a}_{i,g-1}$, and fitness $f(\cdot)$ and adaptively compute ω, μ_1 and μ_2. Suppose $\mathbf{o}_k$ be the current observation of a dynamic system at time k, these variables are adaptively computed:

$$\mathbf{a}_{i,g-1} = \Gamma(\mathbf{o}_k, \mathbf{o}_{k-1}), \tag{6}$$

$$f(\mathbf{x}_{i,g}) = p(\mathbf{o}_k | \mathbf{x}_{i,g}), \tag{7}$$

$$\mu_1 = \frac{2p(\mathbf{o}_k | \mathbf{b}_{i,g-1})}{p(\mathbf{o}_k | \mathbf{b}_{i,g-1}) + p(\mathbf{o}_k | \mathbf{c}_{g-1})}, \tag{8}$$

$$\mu_2 = \frac{2p(\mathbf{o}_k | \mathbf{c}_{g-1})}{p(\mathbf{o}_k | \mathbf{b}_{i,g-1}) + p(\mathbf{o}_k | \mathbf{c}_{g-1})}, \tag{9}$$

where function Γ calculates the speed between $\mathbf{o}_k$ and $\mathbf{o}_{k-1}$ and fitness $f(\cdot)$ is defined as observation probability $p(\cdot)$ of each individual relative to current observation $\mathbf{o}_k$. As a matter of fact, the cognitive coefficients are typically close to 2.0, which represents the step size that the individual takes toward the global best candidate solution the swarm has found up until that point [24]. Our adaptive computation follows this fact.

To adaptively determine ω, we define a spatial distribution factor γ_{g-1} at generation $g-1$ on the basis of average distance $d_{i,g-1}$ from $\mathbf{x}_{i,g-1}$ to all the other individuals:

$$d_{i,g-1} = \frac{1}{N-1} \sum_{i=1, i \neq j}^{N} \left\| \mathbf{x}_{i,g-1} - \mathbf{x}_{j,g-1} \right\|, \tag{10}$$

where each individual $\mathbf{x}_{i,g-1}$ contains its own 3-D position and movement orientation information in the search space.

Based on the maximal and minimal distances (d_{max}, d_{min}) from $\{d_{i,g-1}\}_{i=1}^{N}$ and the average distance d_c between the global best $\mathbf{c}_{g-1}$ and $\{\mathbf{x}_{i,g-1}\}_{i=1}^{N}$, the spatial distribution factor γ_{g-1} is adaptively calculated at generation $g-1$ by

$$\gamma_{g-1} = (d_c - d_{min})/(d_{max} - d_{min}), \quad \gamma_{g-1} \in [0,\ 1]. \tag{11}$$

Since coefficient ω usually ranges in the interval $[0.4, 0.9]$ to weight the global and the local searching abilities [24], we use the distribution factor γ_{g-1} and fitness $f(\mathbf{x}_{i,g-1})$ to adaptively calculate the inertial weight ω for controlling the speed $\mathbf{a}_{i,g}$:

$$\omega = \frac{2}{2 + 3\exp(-1.28(p(\mathbf{o}_k | \mathbf{x}_{i,g-1}) + \gamma_{g-1}))}, \tag{12}$$

which shows a novel strategy to automatically control ω. Generally, the inertial weight ω can either dampen the individual's inertia or accelerate the individual in its original direction. While lower values of the inertial weight speed up the convergence of the swarm to optima, higher values of the inertial weight encourage exploration of the entire search space [24]. Eq. (12) is an adaptive method to estimate ω.

Eventually, the output of adaptive particle swarm optimization is the optimal solution $\mathcal{Q}^k$ with respect to the maximal fitness at time k after G iterations:

$$\mathcal{Q}^k = \arg\max_{\mathbf{c}_g \in \mathcal{C}_G} f(\mathbf{c}_g), \tag{13}$$

where $\mathcal{C}_G = \{\mathbf{c}_g\}_{g=1}^G$ is a set of the global general best individuals obtained from each generation after updating.

B. Observation-Boosted Differential Evolution

Differential evolution seeks for the optimal solution by calculating the difference of solution vectors to create new candidates. It is a stochastic parallel search optimization algorithm that is easily implemented and reasonably robust. In differential evolution, three steps are implemented: (1) mutation, (2) crossover, and (3) selection. Our idea is still to integrate the current observation into these steps.

1) Mutation: The differential evolution performance depends heavily on the mutation operator. Such an operator determines the mutant vector $\mathbf{v}_{i,g}$ for the individual or vector $\mathbf{x}_{i,g}$ at generation g by

$$\mathbf{v}_{i,g} = \mathbf{x}_{i,g} + m_i \overbrace{(\mathbf{c}_g - \mathbf{x}_{i,g})}^{\tilde{\pi}_{i,g}} + m_i \overbrace{(\mathbf{x}_{r_i^1,g} - \mathbf{x}_{r_i^2,g})}^{\hat{\pi}_{i,g}}, \tag{14}$$

where m_i denotes the mutation factor, indexes r_i^1 and r_i^2 are mutually exclusive integers selected randomly from set $\{1, \cdots, i-1, i+1, \cdots, N\}$. The mutation operator generally results in good convergence performance since the global best individual $\mathbf{c}_g$ is employed during optimization.

Unfortunately, the best individual $\mathbf{c}_g$ possibly leads to the poor diversity of the population, which causes unstable or premature convergence. This also implies that the population is converged too early to be suboptimal. To resolve the premature convergence problem, we re-formulate this operator and adaptively calculate two mutant factors by the current observation $\mathbf{o}_k$:

$$\mathbf{v}_{i,g} = \mathbf{x}_{i,g} + \underbrace{\alpha_i \Gamma(\mathbf{o}_k, \mathbf{o}_{k-1})}_{observation} + \tilde{m}_i \tilde{\pi}_{i,g} + \hat{m}_i \hat{\pi}_{i,g}, \tag{15}$$

$$\tilde{m}_i = \frac{2p(\mathbf{o}_k|\mathbf{c}_g)}{p(\mathbf{o}_k|\mathbf{x}_{i,g}) + p(\mathbf{o}_k|\mathbf{c}_g)}, \tag{16}$$

$$\hat{m}_i = \frac{2p(\mathbf{o}_k|\mathbf{x}_{i,g})}{p(\mathbf{o}_k|\mathbf{x}_{i,g}) + p(\mathbf{o}_k|\mathbf{c}_g)}, \tag{17}$$

where the random number α_i controls to preserve the current observation and yields an uniform distribution $\alpha_i \in [0, 1]$.

2) Crossover: After the mutation step, a binomial crossover operation is to compute the trial vector $\mathbf{u}_{i,g} = \{u_{i,g}^1, \cdots, u_{i,g}^D\}$ on the basis of the individual vector $\mathbf{x}_{i,g} = \{x_{i,g}^1, \cdots, x_{i,g}^D\}$ and the mutation vector $\mathbf{v}_{i,g} = \{v_{i,g}^1, \cdots, v_{i,g}^D\}$:

$$u_{i,g}^j = \begin{cases} v_{i,g}^j & \text{if } (\delta \le C_r) \text{ or } (j = j_r) \\ x_{i,g}^j & \text{otherwise} \end{cases}, \tag{18}$$

where the random number $\delta \in [0, 1]$, the integer j_r is randomly selected from set $\{1, 2, \cdots, D\}$, and the crossover rate C_r is adaptively computed to check if $u_{i,g}^j$ is copied from $v_{i,g}^j$:

$$C_r = \frac{p(\mathbf{o}_k|\mathbf{x}_{i,g}) + p(\mathbf{o}_k|\mathbf{v}_{i,g})}{2}, \tag{19}$$

Algorithm 1: APSO for surgical navigation

Input: Video images, EM sensor outputs, CT images
Output: A series of endoscopic camera pose $(\mathbf{t}_*^k \ \mathbf{q}_*^k)$

❶ Initialize $\{\mathbf{x}_{i,0}\}_{i=1}^N$, $\{\mathbf{b}_{i,0}\}_{i=1}^N$, and $\mathbf{c}_0$ on the basis of EM sensor measurement $\hat{\mathbf{o}}_1$ at $k = 1$ and set $\hat{\mathbf{o}}_1 = \hat{\mathbf{o}}_0$;
for $k = 1$ **to** K (Frame or measurement number) **do**
  for $g = 1$ **to** G (Generation number) **do**
    ❷ Update fitness by Eq. (25);
    for $i = 1$ **to** N (Population number) **do**
      ❸ Compute μ_1, μ_2, ω, $\mathbf{a}_{i,g}$ by Eqs. (8), (9), (12), and (23);
      ❹ Propagate individual $\mathbf{x}_{i,g}^k$ by Eq. (1);
    end
    ❺ Calculate fitness of $\{\mathbf{x}_{i,g}^k\}_{i=1}^N$ by Eq. (25);
    ❻ Update $\mathbf{b}_i$ and $\mathbf{c}_g$ by Eqs. (4) and (5);
    ❼ Store $\mathbf{c}_g$ in $\mathcal{C}_G$;
    $g = g + 1$;
  end
  ❽ Get current best estimate $(\mathbf{t}_*^k \ \mathbf{q}_*^k)$ by Eq. (26);
  $k = k + 1$;
end

3) Selection: This step updates the population at generation $g+1$ from $\{\mathbf{x}_{i,g}\}_{i=1}^N$ to $\{\mathbf{x}_{i,g+1}\}_{i=1}^N$ using two vector sets of $\{\mathbf{x}_{i,g}\}_{i=1}^N \cup \{\mathbf{u}_{i,g}\}_{i=1}^N$ in accordance with their fitness values:

$$\mathbf{x}_{i,g+1} = \begin{cases} \mathbf{u}_{i,g} & \text{if } f(\mathbf{u}_{i,g}) \ge f(\mathbf{x}_{i,g}) \\ \mathbf{x}_{i,g} & \text{otherwise} \end{cases}. \tag{20}$$

Finally, after the G-th iteration or generation at time k, the output of the observation-boosted differential evolution approach to solve any dynamic optimization problems is the global best solution $\mathcal{Q}^k$ determined by

$$\mathcal{Q}^k = \arg\max_{\mathbf{x}_{i,G} \in \mathcal{X}_G} p(\mathbf{o}_k|\mathbf{x}_{i,G}), \tag{21}$$

where $\mathcal{X}_G = \{\mathbf{x}_{i,G}\}_{i=1}^N$ is a set of evolutionary individuals that are optimized at the final iteration or generation.

IV. Application to Surgical Navigation

This section formulates surgical navigation as the adaptive particle swarm optimization and observation-boosted differential evolution procedures. Surgical navigation refers to accurately track or navigate surgical instruments to target regions in the body during minimally invasive surgery. Endoscopic navigation procedures typically use various devices of an endoscope integrated with video cameras at its distal tip, an EM tracking system, and a computed tomography (CT) scanner. These devices provide endoscopic video sequences, EM sensor measurements, and CT images, respectively. Navigation paths consist of a large sequence of EM sensor measurements that contain a series of 3-D positions and orientations when surgeons move the surgical endoscope integrated with an EM sensor inside the body. In this respect, each EM sensor measurement corresponds or maps to the individual defined in the modified evolutionary optimization algorithms. Based on these

Algorithm 2: OBDE for surgical navigation

Input: Video images, EM sensor outputs, CT images
Output: A series of endoscopic camera pose $(\mathbf{t}_*^k\ \mathbf{q}_*^k)$

❶ Initialize $\{\mathbf{x}_{i,0}\}_{i=1}^N$ and $\mathbf{c}_0$ on the basis of EM sensor measurement $\hat{\mathbf{o}}_1$ at $k=1$ and set $\hat{\mathbf{o}}_1 = \hat{\mathbf{o}}_0$;
for $k = 1$ **to** K (Frame or measurement number) **do**
  for $g = 1$ **to** G (Generation number) **do**
    ❷ Update fitness by Eq. (25);
    for $i = 1$ **to** N (Population number) **do**
      ❸ Compute $\tilde{m}_i$, $\hat{m}_i$, C_r, and observation by(Eqs. (16), (17), and (14);
      ❹ New mutation to get $\mathbf{v}_{i,g}^k$ Eq. (15);
      ❺ Crossover to get $\mathbf{u}_{i,g}^k$ Eq. (18);
      ❻ Selection by Eqs. (20) and (25);
    end
    $g = g + 1$;
  end
  ❼ Obtain population $\{\mathbf{x}_{i,G}^k\}_{i=1}^N$;
  ❽ Find current best estimate $(\mathbf{t}_*^k\ \mathbf{q}_*^k)$ by Eq. (26);
  $k = k + 1$;
end

data, the question of surgical navigation is to continuously and precisely estimate the current endoscopic camera pose including position and orientation in the CT image space, i.e., to predict the transformation matrix from the endoscopic camera to the CT image coordinate system.

Suppose that $\mathbf{t}^k$ and quaternion $\mathbf{q}^k$ represents the endoscopic camera position and orientation, respectively. In APSO or OBDE, $\mathbf{x}_{i,g}$ becomes $\mathbf{x}_{i,g}^k$ that is a seven-dimensional vector ($D = 7$) including position $\mathbf{t}^k$ and quaternion $\mathbf{q}^k$:

$$\mathbf{x}_{i,g}^k = \left(\mathbf{t}^k\ \mathbf{q}^k\right) = (t_x^k, t_y^k, t_z^k, q_0^k, q_1^k, q_2^k, q_3^k), \tag{22}$$

where t_x^k, t_y^k, t_z^k are the position in the x-, y-, and z-axes of the CT coordinates and $(q_0^k)^2 + (q_1^k)^2 + (q_2^k)^2 + (q_3^k)^2 = 1$. Note that we use quaternions but not rotation matrices to present endoscopic camera orientation in our implementation. While Quaternions are a number system including a wide and complex mathematical theory and only describe rotation, they provide rotation with several advantages, e.g., obvious geometrical interpretation, coordinate system independence and compact representation, to characterize endoscope three directions and save their storage space [26].

The inputs of the adaptive particle swarm optimization and observation boosted differential evolution approaches are endoscopic images, EM sensor measurements, and CT images in the navigation procedure. The current observation $\mathbf{o}_k$ includes the endoscopic image $\tilde{\mathbf{o}}_k$ and the EM sensor measurement $\hat{\mathbf{o}}_k$ at frame k. CT images and volume rendering techniques are used to generate 2-D virtual rendering image $\mathbf{I}(\mathbf{x}_{i,g}^k)$ corresponding to individual $\mathbf{x}_{i,g}^k$. In the optimization procedures, $\Gamma(\cdot)$ presented in Eqs. (6) and (15) is calculated in accordance with EM sensor measurements $\hat{\mathbf{o}}_k$ and $\hat{\mathbf{o}}_{k-1}$:

$$\Gamma(\hat{\mathbf{o}}_k, \hat{\mathbf{o}}_{k-1}) = \hat{\mathbf{o}}_k - \hat{\mathbf{o}}_{k-1}. \tag{23}$$

The fitness value $f(\cdot)$ of each individual $\mathbf{x}_{i,g}^k$ is computed:

$$f(\mathbf{x}_{i,g}^k) = p(\tilde{\mathbf{o}}_k|\mathbf{x}_{i,g}^k) = s(\tilde{\mathbf{o}}_k, \mathbf{I}(\mathbf{x}_{i,g}^k)), \tag{24}$$

where the similarity $s(\tilde{\mathbf{o}}_k, \mathbf{I}(\mathbf{x}_{i,g}^k))$ between the video image $\tilde{\mathbf{o}}_k$ and virtual rendering image $\mathbf{I}(\mathbf{x}_{i,g}^k)$ is defined as [27]:

$$s(\tilde{\mathbf{o}}_k, \mathbf{I}(\mathbf{x}_{i,g}^k)) = \frac{(2\xi_k\xi_i + C_1)\,(2\delta_{k,i} + C_2)}{(\xi_k^2 + \xi_i^2 + C_1)\,(\delta_k^2 + \delta_i^2 + C_2)}, \tag{25}$$

where $\delta_{k,i}$ is the correlation between images $\tilde{\mathbf{o}}_k$ and $\mathbf{I}(\mathbf{x}_{i,g}^k)$; ξ_k and ξ_i are the average intensity values; δ_k and δ_i denote the intensity variances, and C_1 and C_2 are two constants.

Finally, according to Eqs. (13) and (21), the APSO-based and OBDE-driven navigation methods determine the optimal estimate for the current endoscopic camera pose $(\mathbf{t}_*^k\ \mathbf{q}_*^k)$ by

$$\left(\mathbf{t}_*^k\ \mathbf{q}_*^k\right) = \begin{cases} \arg\max_{\{\mathbf{c}_g^k\}_{g=1}^G} p(\tilde{\mathbf{o}}_k|\mathbf{c}_g^k) & \text{APSO} \\ \arg\max_{\{\mathbf{x}_{i,G}^k\}_{i=1}^N} p(\tilde{\mathbf{o}}_k|\mathbf{x}_{i,G}^k) & \text{OBDE} \end{cases}. \tag{26}$$

Our proposed adaptive particle swarm optimization and observation-boosted differential evolution algorithms to track the endoscope motion for surgical navigation are summarized in Algorithm 1 and Algorithm 2.

As shown in Algorithm 1 and Algorithm 2, our modified evolutionary optimization algorithms to estimate endoscopic camera pose at k-th frame are automatically terminated after G iterations or generations. At each iteration, we select the optimal solution $\mathbf{c}_g$ from the updated local individual best set $\{\mathbf{b}_{i,g}\}_{i=1}^N$ and store $\mathbf{c}_g$ in set $\mathcal{C}_G = \{\mathbf{c}_g\}_{g=1}^G$. Eventually, we determine the global best solution by comparing all the optimal solutions in $\mathcal{C}_G$ in term of their fitness (Eq. (26)).

In addition, our algorithms require to initialize individual $\mathbf{x}_{i,0}$ in the population at generation 0 before iteration. In our case, each individual $\mathbf{x}_{i,0}$ is initialized as the first EM sensor measurement $\hat{\mathbf{o}}_1$ (i.e., at frame $k=1$): $\mathbf{x}_{i,0} = \mathbf{b}_{i,0} = \mathbf{c}_0 = \hat{\mathbf{o}}_1$. We also set $\hat{\mathbf{o}}_1 = \hat{\mathbf{o}}_0$ in the first iteration.

V. Experimental Settings

We built a rubber bronchial tree phantom model (Fig. 2(a)) to evaluate our proposed methods. In phantom experiments, we employed a 3-D Guidance medSAFE tracker (Ascension Technology Corporation, USA) as the electromagnetic tracking system at a frame rate of 30 Hz (Fig. 2(b)), which includes an EM sensor and a 9-coil flat type transmitter as a magnetic field generator. In addition, a flexible endoscope (BF-P260F, Olympus, Tokyo, Japan) was used to acquire endoscopic video images of size 362×370 pixels at a frame rate of 30 frames per second. The electromagnetic sensor was fixed at the distal tip of the flexible endoscope that was manipulated by the surgeon flying through the mouth or nose to the bronchial tree of the patient or the phantom. The electronic unit and magnetic field generator perceive and measure the position and orientation of the EM sensor to track real-time movement of the flexible endoscope. All the experiments were tested on a laptop installed with Windows 8.1 Professional 64-Bit System, 32.0-GB Memory, and Processor Intel Xeon CPU×8 and were implemented in Microsoft Visual Studio C++ 2008.

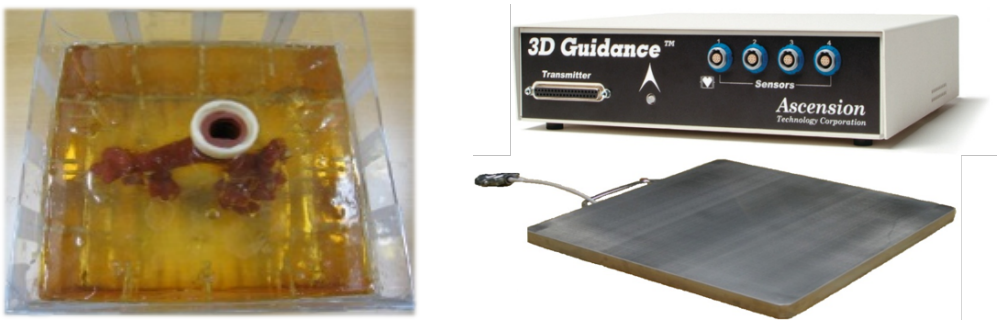

(a) Phantom (b) EM tracking system

Fig. 2: A built phantom and an EM system with electronic unit and flat-type magnetic field generator used in our experiments

TABLE I: Position and orientation errors, processing time per frame, and visual quality of using different methods.

Approaches	Position (mm)	Orientation (°)	Time (second)	Visual quality
Mori et al. [4]	4.84±4.73	9.82±4.74	0.31	0.658
Soper et al. [5]	4.38±3.80	9.24±5.48	1.59	0.664
APSO	3.33±2.41	9.63±4.24	0.99	0.698
OBDE	2.92±2.62	9.37±4.12	0.67	0.724

Based on these devices and systems discussed above, six datasets of endoscopic video sequences, EM sensor measurements, and CT images were collected to validate the APSO- and OBDE-based navigation methods. We manually generated ground truth for these data and computed position and orientation errors between ground truth and endoscopic camera pose estimates. While the ground-truth data were created by adjusting the position and orientation of the virtual endoscopic camera to qualitatively align the real and virtual viewing points by hand, they were independently and repeatedly generated in multiple sessions by three observers, one bronchoscopist and two scientists. These sessions involve extreme amount of manual labor. On the other hand, we also define the visual quality as the similarity of endoscopic video images and their corresponding 2-D virtual rendering images generated using endoscopic camera pose estimates in the CT images.

We compare four methods: (1) Mori et al. [4], directly combining EM sensor measurements and endoscopic videos to estimate camera motion, (2) Soper et al. [5], a hybrid method of using endoscopic video images and EM sensor measurements with Kalman filtering, and (3) adaptive particle swarm optimization (APSO), and (4) observation-boosted differential evolution (OBDE), as discussed in Sections III and IV. Note that we experimentally determine the population size and generation number (G, N) of APSO and OBDE as $(8, 20)$ and $(2, 25)$, which also are their termination criteria.

VI. Results

Table I quantifies the navigation position and orientation errors, processing time, and visual quality of using different methods. While a clinical requirement of surgical navigation is about 3.0 mm for endoscopic surgery, the adaptive particle swarm optimization and observation-boosted differential evolution methods provide an error of 3.33 mm and 2.92 mm, respectively, which were much better than the previous hybrid methods [4], [5]. Note that the previous hybrid approaches commonly use deterministic optimization [4], [5] and generally perform much better than only directly using EM measurements for surgical navigation. This work focuses on evolutionary computation to optimize EM sensor measurements. Our evolutionary optimization-based surgical navigation frameworks generally outperform the previous hybrid methods that use deterministic optimization [4], [5].

The computational times of the adaptive particle swarm optimization and observation-boosted differential evolution approaches were about 0.99 and 0.67 seconds per frame, respectively. The processing time depends heavily on the generation number and fitness computation. Graphic processing unit techniques can speed up the proposed methods to meet the real-time requirement of surgical navigation.

Fig. 3 plots examples of the navigation results. While the navigation results are a series of numbers that represent the endoscope's position and orientation in the CT space, they are meaningless to surgeons who have difficulty in interpreting these numbers properly in the operating room. The surgeon expects to directly and intuitively visualize the navigation results whether they are accurate or not. Fortunately, virtual endoscopic images can be generated by volume rendering on the basis of these numbers and CT images. These generated virtual rendering images are clinically meaningful to surgeons. Fig. 4 visually compares virtual rendering images of using the four different methods. To identify the best performance of the four methods, we directly inspect how the generated virtual rendering images are similar to the real input endoscopic images. The more similar between the real image and virtual rendering image generated by a method, the better performance of the method. All these virtual rendering results demonstrate that two modified evolutionary computation algorithms of adaptive particle swarm optimization and observation-boosted differential evolution improve the navigation performance.

VII. Discussion

The objective of this work is to resolve the problems in EM sensor measurements when using EM tracking sys-

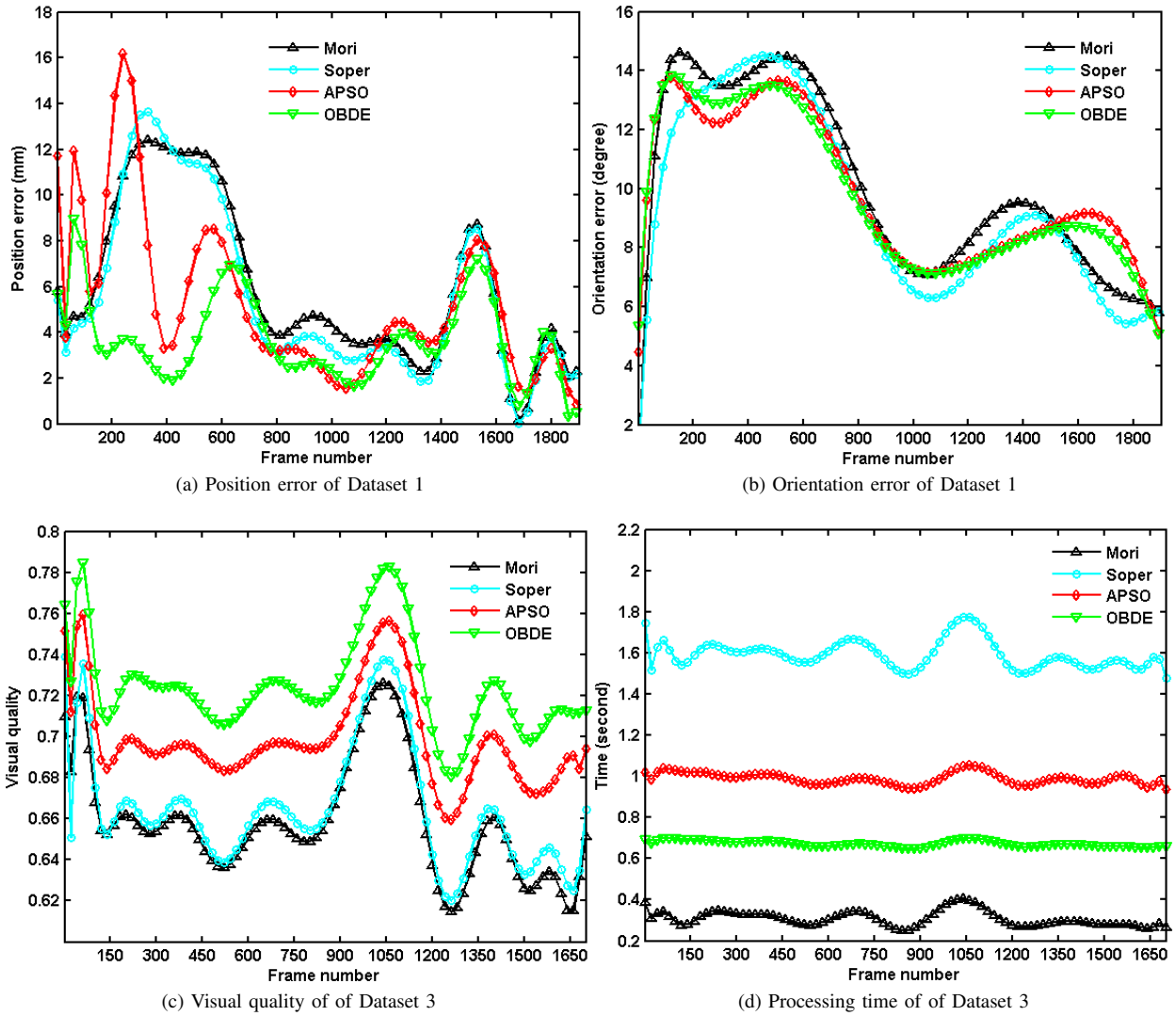

(a) Position error of Dataset 1

(b) Orientation error of Dataset 1

(c) Visual quality of of Dataset 3

(d) Processing time of of Dataset 3

Fig. 3: Examples of plotted navigation errors, processing time per frame, and visual quality of using different methods.

tems for surgical navigation. We proposed an evolutionary optimization-based strategy to improve the accuracy of the EM sensor outputs and the performance of surgical navigation. Several interesting technical aspects are contributed to such an improvement.

First, old individuals in the population are propagated to new individuals by using the current observation of the EM sensor, which generally prevents APSO and OBDE from being trapped in a local optimum. The current observation information is important to positively guide these individuals to approximate the optimal solution for the current endoscopic camera's position and orientation since such information indicates the current state of the endoscope movement. Second, evolutionary factors play an essential role in the APSO and OBDE methods. We automatically determined these factors on the basis of the fitness of each individual in the adaptive particle swarm optimization and observation-boosted differential evolution methods, which were beneficial to avoid the premature convergence of evolutionary computation. Next, the fitness of individuals was also computed in accordance with the current endoscopic image information, resulting in improving the exploration of the individual. Moreover, OBDE works generally better than APSO (Fig. 3). This is because that the diversity of the population in OBDE using the mutation and crossover operators is better than APSO. Also note that the computational time of APSO or OBDE processing each frame was similar because all the images were the same size.

Although the adaptive particle swarm optimization and observation-boosted differential evolution methods work well and improve inaccurate and uncertain EM sensor measurements for robust surgical navigation, they have several potential limitations. First, the proposed methods do not guarantee to completely resolve problematic EM sensor measurements. The magnetic field distortion is an inherent drawback and still an open issue when using EM tracking systems for surgical navigation. Next, the fitness computation of the population plays an important role during optimization. Our fitness computation has two drawbacks: (1) it depends on the quality of endoscopic video images and (2) it possibly increases the computational complexity. Endoscopic videos usually contain

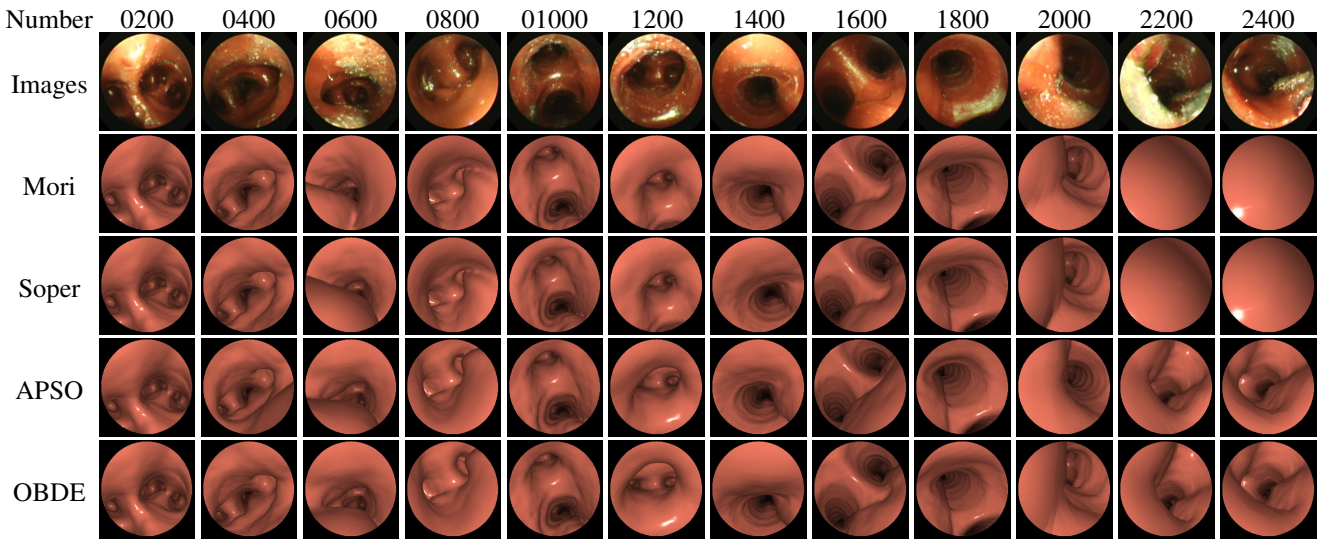

Fig. 4: Examples of visual comparison of camera pose estimates on Dataset 6. Top row shows frame numbers and second row their corresponding video images. Other rows display virtual rendering images generated from estimates of different methods. A method outperforms another if video images resemble better to virtual rendering ones. OBDE shows the best performance.

image artifacts that definitely influence the accuracy of the fitness. In addition, calculating the similarity (fitness) is generally a time-consuming processing. We can employ graphics processing unit techniques to accelerate our processing to meet the performance of real-time clinical requirement.

VIII. Conclusions

This work proposes to evolutionarily optimize real-time electromagnetic sensor measurements in electromagnetic tracking systems. We modified two evolutionary optimization methods and developed the adaptive particle swarm optimization and observation-boosted differential evolution algorithms to boost surgical navigation. The experimental results demonstrated that the adaptive particle swarm optimization and observation-boosted differential evolution approaches provide more effective strategies to improve the navigation accuracy. In particular, the observation-boosted differential evolution outperforms the adaptive particle swarm optimization. Future work includes further development of optimization, accurate calculation of fitness, and reduction of computational time.

References

[1] S. Song, Z. Li, M. Meng, H. Yu, and H. Ren, "Real-time shape estimation for wire-driven flexible robots with multiple bending sections based on quadratic bezier curves," *IEEE Sensors Journal*, vol. 15, no. 11, pp. 6326–6334, 2015.

[2] C. Shi, X. Luo, P. Qi, T. Li, S. Song, Z. Najdovski, T. Fukuda, and H. Ren, "Shape sensing techniques for continuum robots in minimally invasive surgery: A survey," *IEEE Transactions on Biomedical Engineering*, vol. 64, no. 8, pp. 1665 – 1678, 2017.

[3] A. M. Franz, T. Haidegger, W. Birkfellner, K. Cleary, T. M. Peters, and L. Maier-Hein, "Electromagnetic tracking in medicine – a review of technology, validation, and applications," *IEEE Transactions on Medical Imaging*, vol. 33, no. 8, pp. 1702–1725, 2014.

[4] K. Mori, D. Deguchi, K. Akiyama, T. Kitasaka, C. R. Maurer Jr., Y. Suenaga, H. Takabatake, M. Mori, and H. Natori, "Hybrid bronchoscope tracking using a magnetic tracking sensor and image registration," in *Proc. MICCAI*, vol. LNCS 3750, 2005, pp. 543–550.

[5] T. D. Soper, D. R. Haynor, R. W. Glenny, and E. J. Seibel, "In vivo validation of a hybrid tracking system for navigation of an ultrathin bronchoscope within peripheral airways," *IEEE Transactions on Biomedical Engineering*, vol. 57, no. 3, pp. 736–745, 2010.

[6] T. Reichl, J. Gardiazabal, and N. Navab, "Electromagnetic servoing – a new tracking paradigm," *IEEE Transaction on Medical Imaging*, vol. 32, no. 8, pp. 1526 – 1535, 2013.

[7] X. Luo and K. Mori, "Robust endoscope motion estimation via an animated particle filter for electromagnetically navigated endoscopy," *IEEE Transactions on Biomedical Engineering*, vol. 61, no. 1, pp. 85–95, 2014.

[8] H. Sadjadi, K. Hashtrudi-Zaad, and G. Fichtinger, "Simultaneous electromagnetic tracking and calibration for dynamic field distortion compensation," *IEEE Transactions on Biomedical Engineering*, 2016.

[9] H. Sorger, E. F. Hofstad, T. Amundsen, T. Lango, and H. O. Leira, "A novel platform for electromagnetic navigated ultrasound bronchoscopy (EBUS)," *International Journal of Computer Assisted Radiology and Surgery*, vol. 11, no. 8, pp. 1431–1443, 2016.

[10] E. F. Hofstad, H. Sorger, J. B. L. Bakeng, L. Gruionu, H. O. Leira, T. Amundsen, and T. Lango, "Intraoperative localized constrained registration in navigated bronchoscopy," *Medical Physics*, vol. 44, no. 8, pp. 4204–4212, 2017.

[11] P. J. Reynisson, E. F. Hofstad, H. O. Leira, C. Askeland, T. Lango, H. Sorger, and F. Lindseth, "A new visualization method for navigated bronchoscopy," *Minimally Invasive Therapy &Allied Technologies*, vol. 27, no. 2, pp. 119–126, 2018.

[12] M. Shen, S. Giannarou, and G.-Z. Yang, "Robust camera localisation with depth reconstruction for bronchoscopic navigation," *International Journal of Computer Assisted Radiology and Surgery*, vol. 10, no. 6, pp. 801–813, 2015.

[13] M. Shen, S. Giannarou, P. Shah, and G.-Z. Yang, "Branch: Bifurcation recognition for airway navigation based on structural characteristics," in *Proc. MICCAI*, vol. 10434, 2017, pp. 182–189.

[14] P. D. Byrnes and W. E. Higgins, "Efficient bronchoscopic video summarization," *IEEE Transactions on Biomedical Engineering*, vol. 66, no. 3, pp. 848–863, 2018.

[15] M. McTaggart and W. E. Higgins, "Robust video-frame classification for bronchoscopy," in *Proc. SPIE Medical Imaging*, vol. 10951, 2019, p. 109511Q.

[16] S. Song, H. Ren, and H. Yu, "An improved magnetic tracking method using rotating uniaxial coil with sparse points and closed form analytic solution," *IEEE Senors Journal*, vol. 14, no. 10, pp. 3585–3592, 2014.

[17] Z. Liu, Q. Zhang, M. Pan, F. Guan, K. Xue, and D. Chen, "Compensation of geomagnetic vector measurement system with differential magnetic field method," *IEEE Sensors Journal*, vol. 16, no. 24, pp. 9006–9013, 2016.

[18] S. Su, W. Yang, H. Dai, X. Xia, M. Lin, B. Sun, and C. Hu, "Investigation of the relationship between tracking accuracy and tracking distance of a novel magnetic tracking system," *IEEE Sensors Journal*, vol. 17, no. 15, pp. 4928–4937, 2017.
[19] H. Dai, S. Song, X. Zeng, S. Su, M. Lin, and M. Meng, "6-d electromagnetic tracking approach using uniaxial transmitting coil and tri-axial magneto-resistive sensor," *IEEE Sensors Journal*, vol. 18, no. 3, pp. 1178–1186, 2018.
[20] A. E. Eiben and J. E. Smith, *Introduction to Evolutionary Computing*. Springer, 2007.
[21] J. Kennedy and R. C. Eberhart, "Particle swarm optimization," in *Proc. IEEE Int. Conf. on Neural Networks'95*, 1995, pp. 1942–1948.
[22] R. Storn and K. Price, "Differential evolution - A simple and efficient heuristic for global optimization over continuous spaces," *J. Global Optimi.*, vol. 11, no. 4, pp. 341–359, 1997.
[23] S. Cagnon, E. Lutto, and G. Olagu, *Genetic and Evolutionary Computation for Image Processing and Analysis*. Hindawi Publishing Corporation, 2008.
[24] D. Parrott and X. Li, "Locating and tracking multiple dynamic optima by a particle swarm model using speciation," *IEEE Transactions on Evolutionary Computation*, vol. 10, no. 4, pp. 440–458, 2006.
[25] S. Das and et al., "Differential evolution: A survey of the state-of-the-art," *IEEE Transactions on Evolutionary Computation*, vol. 15, no. 1, pp. 4–31, 2011.
[26] A. J. Hanson, *Visualizing quaternions*. Morgan Kaufmann, 2006.
[27] Z. Wang, A. C. Bovik, H. R. Sheikh, and E. P. Simoncelli, "Image quality assessment: From error visibility to structural similarity," *IEEE Transactions on Image Processing*, vol. 13, no. 4, pp. 600–612, 2004.